AIP | Applied Physics Letters

Selective-area growth and magnetic characterization of MnAs/AlGaAs nanoclusters on insulating Al2O3 layers crystallized on Si(111) substrates

Shinya Sakita, Shinjiro Hara, Matthias T. Elm, and Peter J. Klar

Citation: Applied Physics Letters **108**, 043108 (2016); doi: 10.1063/1.4941082
View online: http://dx.doi.org/10.1063/1.4941082
View Table of Contents: http://scitation.aip.org/content/aip/journal/apl/108/4?ver=pdfcov
Published by the AIP Publishing

Selective-area growth and magnetic characterization of MnAs/AlGaAs nanoclusters on insulating Al_2O_3 layers crystallized on Si(111) substrates

Shinya Sakita,[1] Shinjiro Hara,[1,a)] Matthias T. Elm,[2,3] and Peter J. Klar[2]
[1]*Research Center for Integrated Quantum Electronics, Hokkaido University, North 13 West 8, Sapporo 060-8628, Japan*
[2]*Institute of Experimental Physics I, Justus-Liebig-University Giessen, Heinrich-Buff-Ring 16, 35392 Giessen, Germany*
[3]*Institute of Physical Chemistry, Justus-Liebig-University Giessen, Heinrich-Buff-Ring 17, 35392 Giessen, Germany*

(Received 5 November 2015; accepted 20 January 2016; published online 28 January 2016)

We report on selective-area metal-organic vapor phase epitaxy and magnetic characterization of coupled MnAs/AlGaAs nanoclusters formed on thin Al_2O_3 insulating layers crystallized on Si(111) substrates. Cross-sectional transmission electron microscopy reveals that poly-crystalline γ-Al_2O_3 grains are formed after an annealing treatment of the amorphous Al_2O_3 layers deposited by atomic layer deposition on Si(111) substrates. The $\langle 111 \rangle$ direction of the γ-Al_2O_3 grains tends to be oriented approximately parallel to the $\langle 111 \rangle$ direction of the Si substrate. We observe that hexagonal MnAs nanoclusters on AlGaAs buffer layers grown by selective-area metal-organic vapor phase epitaxy on partially SiO_2-masked Al_2O_3 insulator crystallized on Si(111) substrates are oriented with the c-axis along the $\langle 111 \rangle$ direction of the substrates, but exhibit a random in-plane orientation. A likely reason is the random orientation of the poly-crystalline γ-Al_2O_3 grains in the Al_2O_3 layer plane. Magnetic force microscopy studies at room temperature reveal that arrangements of coupled MnAs nanoclusters exhibit a complex magnetic domain structure. Such arrangements of coupled MnAs nanoclusters may also show magnetic random telegraph noise, i.e., jumps between two discrete resistance levels, in a certain temperature range, which can be explained by thermally activated changes of the complex magnetic structure of the nanocluster arrangements. © *2016 AIP Publishing LLC*. [http://dx.doi.org/10.1063/1.4941082]

The intensive activities addressing the heteroepitaxy of ferromagnetic and III–V compound semiconducting layers (FM III–V hybrids) demonstrate the great interests of the spintronics community in this subject. Due to the compatibility of these two types of materials in the hybrids, the possibility of generating new functionalities arises, which may form the basis for novel spintronic device concepts. Among the FM III–V hybrids, the MnAs/GaAs materials system[1] has gained much attention because NiAs-type MnAs layers and nanoclusters (NC) are ferromagnetic at room temperature or even higher temperatures.[2,3] Magnetic logics were proposed using NiAs-type MnAs thin films on GaAs(001) layers.[4] In addition, the NiAs-type MnAs layers serve as an electrical spin injection source for semiconductors[5] and are used for lateral spin valves.[6] FM III–V hybrids are grown typically by low-temperature molecular beam epitaxy,[7,8] and devices are prepared by using conventional top-down fabrication techniques. Granular hybrids in which ferromagnetic NCs are embedded into semiconducting layers are, in particular, an attractive candidate for the use in future nanospintronic devices because huge magnetoresistance (MR) effects were reported.[8,9] However, the technological applications of these granular hybrids synthesized using such conventional techniques are mainly restricted to macroscopic devices. This is due to the random distribution of the NCs in the host material, e.g., the NC size and the randomness in the mean distance between the NCs, which possibly leads to statistical fluctuations in the device characteristics.[9,10] This issue becomes more severe with increasing the degree of miniaturization and has to be solved in the future on the way towards miniaturized devices. In addition to the efforts of creating FM III–V hybrids, the MnAs thin films including poly-crystals, nanoparticles, and nanowires have also been investigated as candidates for possible spintronic device applications on Si.[11–15] We have developed an approach, the so-called selective-area metal-organic vapor phase epitaxy (SA-MOVPE), where problems due to statistical fluctuations can be avoided. SA-MOVPE is based on the bottom-up formation of single-crystalline ferromagnetic MnAs NCs on defined sites of semiconducting substrates. The SA-MOVPE is promising as it enables us to accurately adjust the size, shape, number, position, and spatial arrangement of the MnAs NCs[16–19] within the hybrids to tune its magnetic and magnetotransport properties.[3,20–22] Ordered planar arrangements of coupled NCs show large MR effects[23] and MR ratios of 300% are predicted by theory.[24] However, it was observed that Mn provided during the NC growth diffused into the undoped semiconducting layers, in which it was incorporated as an acceptor yielding a p-type conductive diluted magnetic semiconducting layer.[3] In particular, in the case of spintronic devices where the functionality (e.g., switching) is based on a transport path through coupled NCs, shunting via the surrounding semiconducting matrix is detrimental and should be avoided. In addition, it is still difficult to grow single-crystalline NCs directly on Si(111) substrates

[a)]Author to whom correspondence should be addressed. Electronic mail: hara@rciqe.hokudai.ac.jp. Tel.: +81-11-706-7170. Fax: +81-11-716-6004.

by SA-MOVPE without any interlayer. The reason is the unintentional MnSi alloy formation near the Si surface under standard SA-MOVPE conditions, in particular, at the relatively high growth temperature of 800 °C for MnAs NCs.[25]

In this letter, we offer a solution to the problem of shunting and report on the formation and magnetic characterization of MnAs NCs on nanostructured AlGaAs buffers grown by SA-MOVPE using a crystallized Al_2O_3 insulating interlayer prepared by atomic layer deposition (ALD) on Si(111) substrates. The use of the Al_2O_3 layers enables us to prevent the unintentional Mn diffusion into the semi-insulating substrate and thus the shunting-channel formation. We previously used the crystallization techniques of amorphous Al_2O_3 layers as interlayers on amorphous glass substrates to promote the nucleation before the AlGaAs growth.[26] It was also reported that amorphous Al_2O_3 layers prepared by ALD crystallized after an annealing treatment at a relatively high temperature.[27–29] Furthermore, the epitaxial growth of semiconductors on Al_2O_3 layers was demonstrated, e.g., GaN growth on Si(111) substrates and InGaN growth on ZnO(0001) substrates with Al_2O_3 interlayers.[30,31] Being able to electrically isolate the NCs grown by SA-MOVPE from the underlying semiconducting layers comprises an important step towards making FM III–V hybrids promising candidates for a use in spintronics. Such NCs can be used as building blocks for future spintronic devices, such as magnetic logics, memories, and sensors, that will be fabricated on semiconducting substrates in a reproducible manner, as discussed in our review paper.[32]

For the SA-MOVPE of the NCs, first, a thin amorphous Al_2O_3 layer was deposited by ALD on a Si(111) substrate at 300 °C with $(CH_3)_3Al$ and H_2O as precursors. The thickness of the amorphous Al_2O_3 layers was approximately 5 nm for the samples studied by cross-sectional transmission electron microscopy (TEM) and 10 nm for the samples used for the SA-MOVPE of the MnAs/AlGaAs NCs. We deposited thicker Al_2O_3 layers (10 nm) for the samples used for the NC growth to ensure that pin-hole free Al_2O_3 layers are obtained after the annealing treatment to prevent the precursors for the AlGaAs and MnAs growth from directly reaching the Si(111) surface. After the deposition, we annealed the Si(111) substrates with the deposited Al_2O_3 layers in N_2 at 900 °C for 3 min in a rapid thermal annealing (RTA) system to crystallize the amorphous Al_2O_3 layers. In the next step, the Al_2O_3 layers crystallized on Si(111) substrates were covered with a pre-patterned growth-inhibiting SiO_2 mask layer using plasma-enhanced chemical vapor deposition, electron beam (EB) lithography, and wet chemical etching by buffered HF (BHF) solution. The first annealing treatment is very important to prevent the etch-off of the Al_2O_3 layers by BHF solution for the substrate preparation process of SA-MOVPE. We experimentally confirmed that there was almost no change in the thickness of the Al_2O_3 layers after the annealing treatment at 900 °C or higher by the etching using BHF solution. (In contrast, as-deposited amorphous Al_2O_3 layers and the Al_2O_3 layers after the annealing treatment in N_2 at 800 °C in the RTA system were etched off by BHF solution.) The thicknesses of SiO_2 mask layers and EB resists deposited on the Al_2O_3/Si(111) substrates were 20 and 100 nm, respectively, for any types of mask openings. Only the EB doses of our EB system, JBX-6300FS, JEOL, in which the accelerating voltage was 100 kV, were optimized depending on the size and shape of the mask openings. As a result of the proximity effect during the EB writing, the mask openings were formed in a regular circular-shape, a diameter of 200 nm, and an elongated line shape, 200 nm wide and 10 μm long. The elongation directions were oriented along one of the Si⟨0–11⟩ directions. For the SA-MOVPE, the estimated partial pressures of $(CH_3)_3Ga$, $(CH_3)_3Al$, and AsH_3 precursors were approximately 2.0×10^{-6}, 3.3×10^{-7}, and 1.2×10^{-3} atm. for the AlGaAs buffer layer growth, and those of $(MeCp)_2Mn$ and AsH_3 were 5.2×10^{-7} and 5.8×10^{-4} atm. for the MnAs NC growth, respectively. Before the buffer layer growth, the samples were annealed a second time at 975 °C for 10 min in H_2 in the MOVPE reactor. Only H_2 was introduced into the reactor during cooling down to 400 °C, prior to growing the AlGaAs buffer layers. At this temperature, the buffer layer growth commenced and lasted for 3 min, before the temperature was raised further to 750 °C where the growth continued for another 3 min. Afterwards, the MnAs NCs were grown at 750 °C for 15 min and formed only on the AlGaAs buffer layers grown on the Al_2O_3 layers in the SiO_2 mask openings.

Morphology of the NCs was investigated by scanning electron microscopy (SEM). Lattice images of the crystallized Al_2O_3 layers were examined by cross-sectional TEM. We characterized the magnetic domains (MD) of the NCs by magnetic force microscopy (MFM) under zero magnetic field, $\boldsymbol{B}$, conditions at room temperature after applying $\boldsymbol{B}$ of 1000 G. Electrical contacts were prepared using EB lithography. Ti (10 nm) and Au (100 nm) were used since these electrode metals form ohmic contacts on MnAs NCs as confirmed by current-voltage characteristics (not shown). The temperature dependence of the resistance, R, of coupled NCs was measured from 110 to 230 K using a He-4 flow cryostat. Due to the high R of the NC investigated (about 0.5 GΩ) and to prevent overheating of the NC, a low DC current (2 nA) was used for the measurements. As discussed later, the NC shows magnetic random telegraph noise (MRTN) in a small temperature range between 145 and 175 K. Thus, the temporal dependence of R was investigated in detail at 152 K where the resistivity jumps observed could be recorded with a good statistics. A $\boldsymbol{B}$ was applied neither before nor during the measurements.

Results of the TEM investigation of the Al_2O_3 layers on Si(111) substrates after the annealing treatment only at 975 °C for 10 min in H_2 in the MOVPE reactor are given in Fig. 1(a). It depicts a cross-sectional TEM lattice image taken with an EB injection perpendicular to one of the {0-11} planes of a Si(111) substrate. Lattice fringes which are approximately parallel to the Si{111} planes are markedly observed in a wide area of the Al_2O_3 layer. It was estimated by fast Fourier transform (FFT) of the observed lattice images that these lattice fringes were attributable to a lattice spacing of 0.46 nm, which is in good agreement with the well-known literature value of 0.456 nm (the JCPDS database) for the γ-Al_2O_3{111} planes. Therefore, it is reasonable to assume that the grains observed in the Al_2O_3 layers are γ-Al_2O_3 crystals. In the case of poly-crystalline γ-Al_2O_3 grains in Al_2O_3 layers deposited on amorphous glass

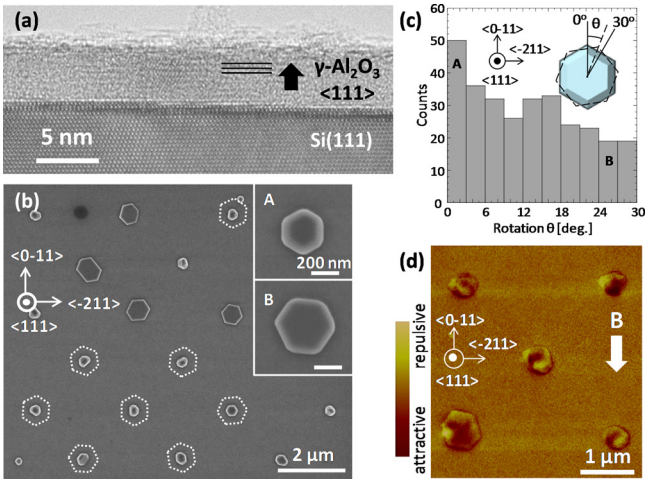

FIG. 1. (a) Cross-sectional transmission electron microscopy lattice image of the sample of a planar 5-nm-thick Al_2O_3 layer deposited on a Si(111) substrate after the AlGaAs growth. (No observable nanostructured AlGaAs buffers on the Al_2O_3 layer are in the observed region.) No SiO_2 mask layer was deposited on the Al_2O_3 layers. (b) Top view of SEM image of the sample after the MnAs growth on AlGaAs nanodisk buffers in the circular SiO_2 mask openings with a diameter of 200 nm. The insets are top views of highly magnified SEM images of typical MnAs NCs. White scale bars in the insets represent 200 nm. (c) Histogram of the rotation angle, θ, distribution for MnAs NCs against the $\langle 0\text{-}11 \rangle$ direction of the Si(111) substrate. (d) Typical magnetic force microscopy image of MnAs NCs grown in regular circular-shaped SiO_2 mask openings with a diameter of 200 nm.

substrates,[26] we observed that some of the γ-$Al_2O_3\{111\}$ planes were titled against the amorphous glass substrate planes. Therefore, we conclude that the γ-$Al_2O_3\langle 111 \rangle$ direction studied here exhibits a marked epitaxial relationship with, i.e., parallel to, the Si$\langle 111 \rangle$ direction. From the BHF etching experiments of Al_2O_3 layers, it appeared that the Al_2O_3 layers were crystallized after the first annealing treatment at 900 °C for 3 min in N_2 in the RTA system, although we have not confirmed that directly by TEM. However, the second annealing treatment at 975 °C for 10 min in H_2 in the MOVPE reactor was carried out to ensure that γ-Al_2O_3 grains were obtained in crystallized Al_2O_3 layers, as shown in Fig. 1(a).

SA-MOVPE of MnAs NCs was carried out just after the SA-MOVPE of the AlGaAs buffer layer on the Al_2O_3/Si(111) substrates covered with a growth-inhibiting SiO_2 mask layer with the regular circular-shape mask openings in the same growth run. Figure 1(b) shows a typical top view of the regular hexagonal NC arrays. We observe that the hexagonal disks are randomly oriented along the Si$\langle 111 \rangle$ direction, as indicated by white dotted hexagons in the figure. The insets show two types of typical NCs marked "*A*" and "*B*." In our previous study on the SA-MOVPE of MnAs NCs on GaAs(111)B substrates,[18] it was found that the hexagons of the NCs, which arise from the hexagonal NiAs-type crystal structure, were always rotated by 30° against those of the AlGaAs buffer layers underneath. The corresponding hexagonal nanodisk structure of the AlGaAs buffer layers exhibits six equivalent {0-11} side-wall facets. (Here, the hexagonal AlGaAs nanodisks, whose estimated diameters were approximately 250 nm or smaller, were not observable as they were covered entirely with the MnAs NCs.) The same holds for NCs of type "*A*" in the inset of Fig. 1(b). Therefore, NCs of type "*A*" possess presumably a similar structure as the NCs grown on GaAs(111)B substrates. In this case, it should be noted that the c-axis of the NCs is parallel to both of the γ-$Al_2O_3\langle 111 \rangle$ and Si$\langle 111 \rangle$ directions. Other NCs, e.g., those of type "*B*," show a different in-plane orientation. We summarized the observed tendency of the NC rotation, θ, against the Si$\langle 0\text{-}11 \rangle$ direction in a histogram shown in Fig. 1(c). The NCs denoted by "*A*" and "*B*" in the insets of Fig. 1(b) represent typical NCs marked in the bars "*A*" and "*B*" in the histogram of Fig. 1(c). The NCs denoted by "*A*" in the inset of Fig. 1(b) show the highest occurrence probability, i.e., 17% (50 counts in the total counts of 294 on the observed samples). We conclude that, in the crystallized Al_2O_3 layers, the $\{111\}$ planes of γ-Al_2O_3 grains are possibly somewhat rotated about the $\langle 111 \rangle$ axis at random despite there is the epitaxial relationship between γ-Al_2O_3 and the Si$\{111\}$ planes. It is also possible that the γ-$Al_2O_3\{111\}$ planes are titled against the Si$\{111\}$ plane. However, the results shown in the histogram seem to be consistent with the cross-sectional TEM investigation results, which confirm that almost all the observed lattice fringes of γ-Al_2O_3 are approximately parallel to the Si$\{111\}$ planes. We conclude that these hexagonal NCs are MnAs as MFM measurements yield a noticeable magnetic response and confirm the MD formation. Figure 1(d) shows a typical MFM image for regular hexagonal-shape NCs recorded at room temperature after applying $\boldsymbol{B} = 1000$ G along the direction indicated by the thick white arrow. We confirmed that the MDs were mostly multi-MDs, although some of the observed small NCs had a single MD.

In the case of the elongated line-like mask openings, we have not obtained uniform lateral MnAs nanowires, but a kind of MnAs NC chain structure with different sizes and shapes aligned parallel to the Si$\langle 0\text{-}11 \rangle$ direction. This might be due to the only partial crystalline character of the Al_2O_3 layers on the length scale of the relatively long elongated mask opening of 10 μm. This appears to be a likely reason because we have observed the lateral MnAs nanowire formation with lengths of 5 μm or longer on single-crystalline AlGaAs buffer layers grown in similar SiO_2 mask openings on GaAs(111)B substrates.[33] As shown in Fig. 2(a), some of the NCs have an elongated or almost regular polygonal shape with well-defined crystal facets, although the size uniformity of the NCs is rather poor, while others are probably poly-crystalline. As reported elsewhere,[27,28] the peak intensities of X-ray diffraction spectra from the crystallized Al_2O_3 layers on Si increased with increasing the annealing temperature, which possibly showed that a better quality of crystallized Al_2O_3 layers with poly-crystalline grains was obtained at higher annealing temperatures. In particular, it was reported that α-Al_2O_3 layers were formed on Si(111) substrates by annealing at temperatures higher than 1050 °C.[28] It was difficult to increase the annealing temperatures further in the current study due to the limitation in our experimental set-up. However, we believe that relatively long lateral MnAs nanowires can be obtained by the present approach as in the case of the SA-MOVPE on GaAs(111)B substrates.[33] Figure 2(b) shows an MFM image of the same structure presented in Fig. 2(a) recorded at room temperature after applying $\boldsymbol{B} = 1000$ G along the direction indicated by the thick

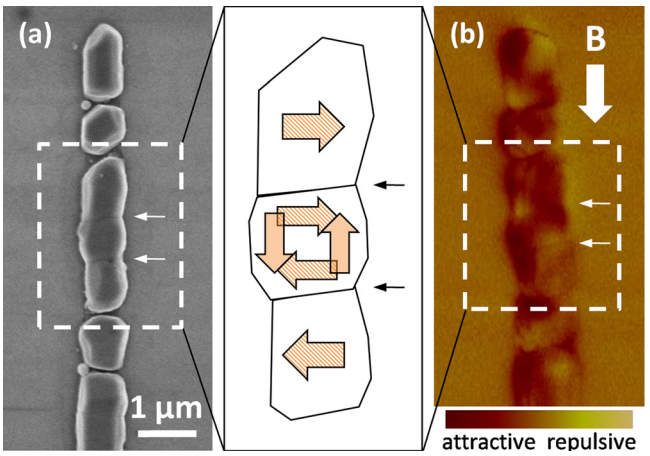

FIG. 2. (a) Scanning electron and (b) magnetic force microscopy images of MnAs NCs grown in an elongated line-shaped SiO_2 mask opening with a width of 200 nm and a length of 10 μm. Two thin white arrows in (a) and (b) and black arrows in the illustration represent the interfaces between the coupled MnAs NCs.

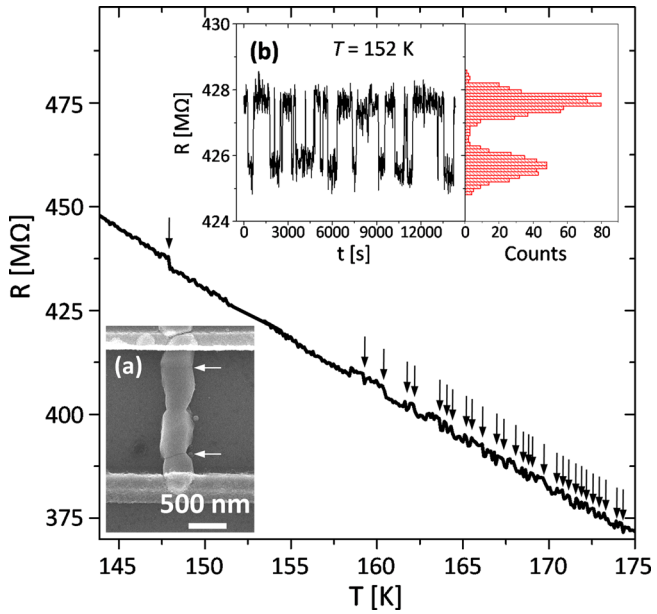

FIG. 3. Temperature dependence of the resistance, R, of coupled MnAs NCs from 145 to 175 K. Black arrows in the figure show the positions at which R jumps between high and low R levels. The inset (a) shows a scanning electron microscopy image of the coupled MnAs NCs measured. Two white arrows in the inset represent the interfaces between the coupled MnAs NCs. The inset (b) shows the observed random telegraph noise of coupled MnAs NCs at a specific temperature of 152 K. The histogram summarizes the count distribution of the R values from the temporal dependence of R at 152 K.

white arrow. For the arrangement consisting of three NCs marked by the white broken rectangle in the middle of Fig. 2(a), we observe four MDs, i.e., a single magnetic domain for each of the outer two NCs and two MDs for the NC in the center of the arrangement. The two thin white arrows in Fig. 2 represent the interfaces between the coupled NCs. For the outer two NCs, it seems that their magnetizations are oriented perpendicular to the $\boldsymbol{B}$ direction; i.e., the applied $\boldsymbol{B}$ strength seems to be insufficient to align the magnetization directions of the NCs. The centered NC with an almost regular polygonal shape seems to consist of two MDs, whose magnetizations are oriented in an anti-parallel configuration. The two possibilities for the anti-parallel alignment are schematically illustrated. Similar complex MDs were observed in the regular hexagonal-shape NCs, as shown in Fig. 1(d), which might depend on the MnAs crystal quality.

Finally, after the two-terminal device fabrication process, we measured the temperature and temporal dependences of R for a small number of coupled MnAs NCs. A top view SEM image of the NC arrangement investigated is shown as the inset (a) of Fig. 3. The arrangement consists of three NCs oriented along the Si⟨0-11⟩ direction, which are located between the two electrodes fabricated. Two NCs exhibit an almost regular polygonal shape while in between two NCs merged during the growth of a long elongated NC with a constriction in its center. Two white arrows in the image denote the possible interfaces between the coupled NCs. The temperature dependence of R confirms that R decreases with increasing the temperature from 110 to 230 K (not shown). Furthermore, as shown in Fig. 3, discrete jumps in R marked by black arrows are observed in a narrow temperature range from 145 to 175 K, which occur more frequently when the temperature is increased. Such resistance fluctuations in nanoscaled magnetic systems typically occur in a small temperature range of 20–30 K and can be attributed to MRTN.[34,35] The inset (b) shows the temporal dependence of R for the coupled NCs at an intermediate temperature of 152 K. The temporal dependence of R as well as the histogram of R levels shown in the inset (b) clearly demonstrates that the NC arrangement exhibits MRTN, where R fluctuates between two discrete R levels. As shown in our previous study,[22] the MRTN can be attributed to thermally activated changes of the magnetic structure of coupled NCs, such as switching of a small MD or thermal fluctuations of the domain wall between different MDs. The observed behavior can be understood qualitatively by assuming that the NC arrangement consists of different MDs, which is in accordance with the MFM observations.[22,33] Assuming a similar MD structure as observed by MFM in the comparable NC arrangement in Fig. 2(b), the NC arrangement investigated may exhibit a complex MD structure, i.e., a single MD for each of the NCs or even two MDs in one single NC. As the outer NC shapes are almost regular polygonal, no strong magnetic shape anisotropy is expected. Assuming single MD character of all the three NCs, the discrete jumps between two R levels shown in Fig. 3 may then be caused by thermally activated changes of the magnetization orientation in the NC with an almost regular polygonal shape or of the domain walls between the MDs, while, for the elongated NC with a constriction in its center, the magnetization may be fixed due to a relatively strong magnetic shape anisotropy. However, a detailed MRTN investigation is needed to establish a complex magnetic structure. We believe that an even better control of the MDs may be achieved after further optimization of the crystallization processes of the Al_2O_3 layers to build MR devices fabricated by our bottom-up approach on Si(111) substrates.

The authors would like to express sincere thanks to M. Fischer, Professor T. Fukui, and Professor J. Motohisa for fruitful and helpful discussion, and R. Kodaira, H. Kato, H. Fujimagari, and Dr. Y. Kohashi for support in the MOVPE

growth experiments. This work was financially supported in part by the Grant-in-Aid for Challenging Exploratory Research (KAKENHI Grant No. 25600034) from the Japan Society for the Promotion of Science (JSPS) and the Japan-Germany Research Cooperative Program from the JSPS and DAAD.

[1]R. Engel-Herbert, T. Hesjedal, D. M. Schaadt, L. Däweritz, and K. H. Ploog, Appl. Phys. Lett. **88**, 052505 (2006).
[2]F. Ishikawa, K. Koyama, K. Watanabe, and H. Wada, Jpn. J. Appl. Phys. **42**, L918 (2003).
[3]M. T. Elm, C. Michel, J. Stehr, D. M. Hofmann, P. J. Klar, S. Ito, S. Hara, and H.-A. Krug von Nidda, J. Appl. Phys. **107**, 013701 (2010).
[4]P. Pampuch, A. K. Das, A. Ney, L. Däweritz, R. Koch, and K. H. Ploog, Phys. Rev. Lett. **91**, 147203 (2003).
[5]M. Ramsteiner, H. Y. Hao, A. Kawaharazuka, H. J. Zhu, M. Kästner, R. Hey, L. Däweritz, H. T. Grahn, and K. H. Ploog, Phys. Rev. B **66**, 081304(R) (2002).
[6]D. Saha, M. Holub, P. Bhattacharya, and Y. C. Liao, Appl. Phys. Lett. **89**, 142504 (2006).
[7]V. Garcia, H. Jaffrès, J.-M. George, M. Marangolo, M. Eddrief, and V. H. Etgens, Phys. Rev. Lett. **97**, 246802 (2006).
[8]S. Sugahara and M. Tanaka, Appl. Phys. Lett. **80**, 1969 (2002).
[9]P. N. Hai, S. Ohya, M. Tanaka, S. E. Barnes, and S. Maekawa, Nature **458**, 489 (2009).
[10]C. Michel, M. T. Elm, B. Goldlücke, S. D. Baranovskii, P. Thomas, W. Heimbrodt, and P. J. Klar, Appl. Phys. Lett. **92**, 223119 (2008).
[11]K. Akeura, M. Tanaka, T. Nishinaga, and J. De Boeck, J. Appl. Phys. **79**, 4957 (1996).
[12]A. M. Nazmul, A. G. Banshchikov, H. Shimizu, and M. Tanaka, J. Cryst. Growth **227–228**, 874 (2001).
[13]M. Solzi, C. Pernechele, M. Ghidini, M. Natali, and M. Bolzan, J. Magn. Magn. Mater. **322**, 1565 (2010).
[14]M. F. H. Wolff, D. Görlitz, K. Nielsch, M. E. Messing, and K. Deppert, Nanotechnology **22**, 055602 (2011).
[15]J. Sadowski, A. Siusys, A. Kovacs, T. Kasama, R. E. Dunin-Borkowski, T. Wojciechowski, A. Reszka, and B. Kowalski, Phys. Status Solidi B **248**, 1576 (2011).
[16]S. Hara, D. Kawamura, H. Iguchi, J. Motohisa, and T. Fukui, J. Cryst. Growth **310**, 2390 (2008).
[17]S. Ito, S. Hara, T. Wakatsuki, and T. Fukui, Appl. Phys. Lett. **94**, 243117 (2009).
[18]K. Komagata, S. Hara, S. Ito, and T. Fukui, Jpn. J. Appl. Phys. **50**, 06GH01 (2011).
[19]S. Hara and K. Komagata, Phys. Status Solidi B **252**, 1925 (2015).
[20]M. T. Elm, P. J. Klar, S. Ito, and S. Hara, Phys. Rev. B **83**, 235305 (2011).
[21]M. T. Elm, P. J. Klar, S. Ito, S. Hara, and H.-A. Krug von Nidda, Phys. Rev. B **84**, 035309 (2011).
[22]M. Fischer, M. T. Elm, H. Kato, S. Sakita, S. Hara, and P. J. Klar, Phys. Rev. B **92**, 165306 (2015).
[23]M. Fischer, M. T. Elm, S. Sakita, S. Hara, and P. J. Klar, Appl. Phys. Lett. **106**, 032401 (2015).
[24]C. Heiliger, M. Czerner, P. J. Klar, and S. Hara, IEEE Trans. Magn. **46**, 1702 (2010).
[25]S. Hara and K. Morita (unpublished).
[26]S. Sakita and S. Hara, Jpn. J. Appl. Phys. **54**, 075504 (2015).
[27]S. Jakschik, U. Schroeder, T. Hecht, M. Gutsche, H. Seidl, and J. W. Bartha, Thin Solid Films **425**, 216 (2003).
[28]L. Zhang, H. C. Jiang, C. Liu, J. W. Dong, and P. Chow, J. Phys. D **40**, 3707 (2007).
[29]C. M. Tanner, M. F. Toney, J. Lu, H. O. Blom, M. Sawkar-Mathur, M. A. Tafesse, and J. P. Chang, J. Appl. Phys. **102**, 104112 (2007).
[30]W. E. Fenwick, N. Li, T. Xu, A. Melton, S. Wang, H. Yu, C. Summers, M. Jamil, and I. T. Ferguson, J. Cryst. Growth **311**, 4306 (2009).
[31]N. Li, S. J. Wang, C. L. Huang, Z. C. Feng, A. Valencia, J. Nause, C. Summers, and I. Ferguson, J. Cryst. Growth **310**, 4908 (2008).
[32]M. T. Elm and S. Hara, Adv. Mater. **26**, 8079 (2014).
[33]H. Kato, S. Sakita, and S. Hara, J. Cryst. Growth **414**, 151 (2015).
[34]F. Coppinger, J. Genoe, D. K. Maude, X. Kleber, L. B. Rigal, U. Gennser, J. C. Portal, K. E. Singer, P. Rutter, T. Taskin, A. R. Peaker, and A. C. Wright, Phys. Rev. B **57**, 7182 (1998).
[35]W. Wernsdorfer, E. B. Orozco, K. Hasselbach, A. Benoit, B. Barbara, N. Demoncy, A. Loiseau, H. Pascard, and D. Mailly, Phys. Rev. Lett. **78**, 1791 (1997).